Insights into the Exfoliation Process of V2O5· nH2O Nanosheet Formation Using Real-Time 51V NMR

(article starts on next page)

Insights into the Exfoliation Process of V₂O₅·nH₂O Nanosheet Formation Using Real-Time ⁵¹V NMR

Ahmed S. Etman,[†,§,#] Andrew J. Pell,[†] Peter Svedlindh,[‡] Niklas Hedin,[†] Xiaodong Zou,[†] Junliang Sun,*[,†,∥] and Diana Bernin*[,†,⊥]

[†]Department of Materials and Environmental Chemistry, Stockholm University, 10691 Stockholm, Sweden

[‡]Department of Engineering Sciences, Uppsala University, 75121 Uppsala, Sweden

[§]Department of Chemistry, Faculty of Science, Alexandria University, Ibrahimia, 21321 Alexandria, Egypt

[∥]College of Chemistry and Molecular Engineering, Peking University, 100871 Beijing, China

[⊥]Department of Chemistry and Chemical Engineering, Chalmers University of Technology, 41296 Gothenburg, Sweden

Ⓢ Supporting Information

ABSTRACT: Nanostructured hydrated vanadium oxides (V₂O₅·nH₂O) are actively being researched for applications in energy storage, catalysis, and gas sensors. Recently, a one-step exfoliation technique for fabricating V₂O₅·nH₂O nanosheets in aqueous media was reported; however, the underlying mechanism of exfoliation has been challenging to study. Herein, we followed the synthesis of V₂O₅·nH₂O nanosheets from the V₂O₅ and VO₂ precursors in real time using solution- and solid-state ⁵¹V NMR. Solution-state ⁵¹V NMR showed that the aqueous solution contained mostly the decavanadate anion [H₂V₁₀O₂₈]⁴⁻ and the hydrated dioxovanadate cation [VO₂·4H₂O]⁺, and during the exfoliation process, decavanadate was formed, while the amount of [VO₂·4H₂O]⁺ remained constant. The conversion of the solid precursor V₂O₅, which was monitored with solid-state ⁵¹V NMR, was initiated when VO₂ was in its monoclinic forms. The dried V₂O₅·nH₂O nanosheets were weakly paramagnetic because of a minor content of isolated V⁴⁺. Its solid-state ⁵¹V signal was less than 20% of V₂O₅ and arose from diamagnetic V⁴⁺ or V⁵⁺. This study demonstrates the use of real-time NMR techniques as a powerful analysis tool for the exfoliation of bulk materials into nanosheets. A deeper understanding of this process will pave the way to tailor these important materials.
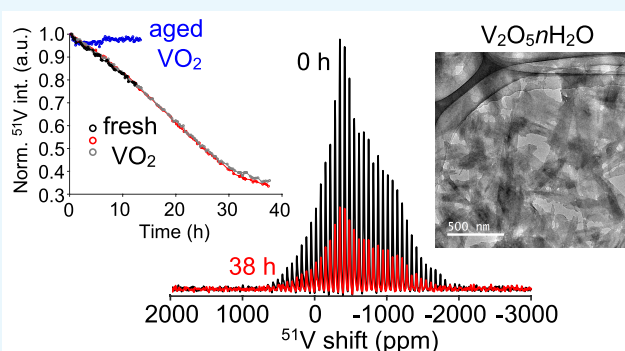
1. INTRODUCTION

In the last few years, the synthesis of two-dimensional (2D) materials based on transition metal chalcogenides and oxides with thicknesses of a few layers has attracted renewed attention because of the different chemical, physical, and semiconducting properties of these materials compared to their bulk (three-dimensional, 3D) counterparts.[1−3] Vanadium oxides are earth-abundant compounds, which have important applications in catalysis,[4] batteries,[5−7] supercapacitors,[8−10] and sensors.[11] Thus, many research groups have focused on the synthesis of 2D vanadium oxides from their bulk precursors.[12−14] Of particular interest among these 2D materials are those based on the hydrated vanadium pentoxides (V₂O₅·nH₂O), which have been shown to exhibit improved electrochemical behavior and semiconducting properties compared to anhydrous V₂O₅.[15] The improvements are typically ascribed to the presence of H₂O or H⁺ ions between the V₂O₅ layers in V₂O₅·nH₂O, which can be synthesized in the form of hydrogels,[16] xerogels,[17,18] nanobelts,[19] and nanosheets.[5−7] Nanostructured V₂O₅·nH₂O has attracted research interest as it can be easily fabricated into a freestanding film,[5] which is easier to handle

than, and is thus advantageous compared to, an amorphous or crystalline powder or gel.

V₂O₅·nH₂O is commonly synthesized either by an ion-exchange route using sodium metavanadate solution or via a sol−gel route using a mixture of hydrogen peroxide (H₂O₂) and V₂O₅.[20,21] In both cases, a dark red compound is formed with a layered structure. Recently, Etman et al. synthetized V₂O₅·nH₂O nanosheets using aqueous exfoliation of a mixture of V₂O₅ and VO₂, resulting in black/green films.[7] The synthesis was monitored by in situ X-ray diffraction (XRD) studies, which revealed that the V₂O₅·nH₂O phase started to form after 90 min of reflux in water at 80 °C. A more detailed understanding of the underlying mechanism of the formation of this V₂O₅·nH₂O product is challenging because vanadium is a transition metal with a very complex chemistry and many different stable oxidation states.[21] As XRD and wide-angle X-ray scattering provide data mainly on the long-range order in

compounds, other techniques are important to assess developments in noncrystalline materials or at the solid–liquid interface during the reaction.

Nuclear magnetic resonance (NMR) is a characterization technique complementary to XRD and has been used to study the ion-exchange or sol–gel synthesis routes of $V_2O_5 \cdot nH_2O$.[22−26] It can provide information about the local order, coordination states, and protonated or deprotonated oxygen atoms. Typically, solid compounds are monitored by magic-angle spinning (MAS) solid-state (ss)-NMR, whereas solution-state NMR is used to observe dissolved compounds. However, both solid- and solution-state ^{51}V NMR are complicated by localized unpaired electrons in paramagnetic V^{4+} ions, which may bleach out the signal arising from the NMR detectable (diamagnetic) $^{51}V^{5+}$ ions in various ways.[27] MAS ss-NMR is able to distinguish between delocalized (metallic) and localized (paramagnetic) electronic states via Knight shifts and paramagnetic shifts.[28] Paramagnetic, which refers here to Curie or Curie–Weiss paramagnetism, V^{4+} ions with localized unpaired electrons cannot be directly studied with NMR, but their presence has the effect of bleaching the ^{51}V signal of nearby V^{5+} ions, allowing the presence of V^{4+} to be probed indirectly. However, V^{4+} ions with localized unpaired electrons can be studied by other techniques, for example, electron spin resonance (ESR). When the V^{4+} ions are less than 2.7 Å apart, their unpaired electrons may pair and turn the corresponding materials from paramagnetic to diamagnetic, which does give a detectable $^{51}V^{4+}$ NMR signal.[27,29,30]

In this paper, we report on real-time solid- and solution-state ^{51}V NMR studies performed during the synthesis of $V_2O_5 \cdot nH_2O$ nanosheets from a 1:4 mixture by weight of commercial monoclinic $VO_2(M)$ and V_2O_5. The interpretation of the ^{51}V NMR results was linked with those from ESR and ^1H NMR and used to elucidate the mechanism of the aqueous exfoliation process and formation of $V_2O_5 \cdot nH_2O$ nanosheets.

2. RESULTS AND DISCUSSION

2.1. Morphology and Structure of $V_2O_5 \cdot nH_2O$ Nanosheets.
The $V_2O_5 \cdot nH_2O$ nanosheets were synthesized in water from a 1:4 mixture by weight of monoclinic $VO_2(M)$ and commercial V_2O_5, and the chemical and thermal analyses are described elsewhere.[7] The XRD pattern (Figure 1a, gray) of the as-prepared $V_2O_5 \cdot nH_2O$ nanosheets displayed broad peaks, which were indexed as 00l, reflecting the preferred orientation of the layered structure of the nanosheets. This pattern was recorded in a reflection configuration using an *in-house* diffractometer (λ = 1.5406 Å). One possible solution to overcome the preferred orientation was to perform XRD in transmission mode with, for example, a high-energy X-ray source (synchrotron radiation, λ = 0.7766 Å). Notably, the XRD pattern (see Figure 1a, black) recorded in this way was very similar to that collected in the reflection mode using an *in-house* diffractometer, suggesting a disordered stacking between $V_2O_5 \cdot nH_2O$ layers over the a–b plane. Interestingly, the transmission electron microscopy (TEM) images showed that $V_2O_5 \cdot nH_2O$ had a typical nanosheet morphology with a different lateral size thickness ranging from 30 to 220 nm (see Figure 1b). In addition, the selected area electron diffraction (SAED) pattern of $V_2O_5 \cdot nH_2O$ had powder rings (see Figure 1c), which provided additional support for disordered stacking between the layers over the a–b plane.

2.1.1. Local Structure of $V_2O_5 \cdot nH_2O$ Nanosheets.
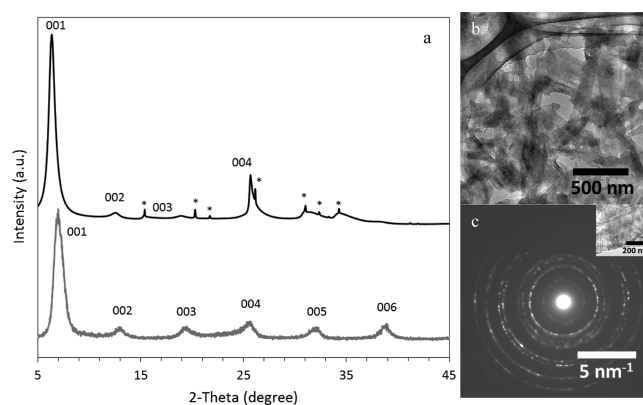MAS ss-NMR can provide fruitful information about the local structure

Figure 1. (a) XRD patterns of $V_2O_5 \cdot nH_2O$ nanosheets in transmission mode using synchrotron radiation (black) and low-energy X-ray reflection (gray) mode. The remaining traces of the V_2O_5 phase are marked by "*". To the right, the TEM image (b) and SAED (c) of the $V_2O_5 \cdot nH_2O$ nanosheets are shown. In (c), the inset shows the crystals from which SAED was obtained.

and oxidation states of metal ions. The commercial V_2O_5 precursor possessed a layered anisotropic structure of distorted VO_6 octahedral building units,[13,31] and its ^{51}V isotropic shift was −611 ppm (see Figure 2, black).[27] The isotropic shift of
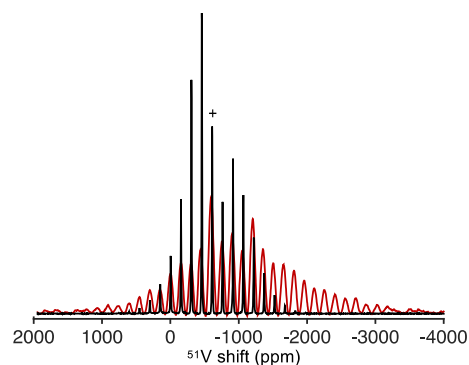

Figure 2. Weight-normalized ^{51}V MAS ss-NMR spectra of V_2O_5 (black) and $V_2O_5 \cdot nH_2O$ nanosheets (red). The signal intensity for $V_2O_5 \cdot nH_2O$ is scaled up by a factor of 20. The isotropic shift is marked by "+".

the largely disordered nanosheets of $V_2O_5 \cdot nH_2O$ was slightly lower in magnitude, −596 ppm, and the spinning side band manifold was broader, having nearly double the number of spinning side bands (see Figure 2, red). In addition, the individual side bands exhibited an increased inhomogeneous line width, which suggested highly distorted geometries of the vanadium sites. The enhanced line width was in agreement with observations from XRD and SAED.

In previous NMR studies of $V_2O_5 \cdot nH_2O$ gels, synthesized using H_2O_2-based or ion-exchange methods, up to five different ^{51}V NMR peaks have been observed and attributed to various vanadium sites.[32,33] The corresponding ^{51}V isotropic shifts have been in the interval of −572 to −663 ppm. However, in this study, the intrinsic and symmetric ^{51}V line width of the ^{51}V NMR peaks of the nanosheets of $V_2O_5 \cdot nH_2O$ exceeded 80 ppm and thus prevented potential multiple vanadium sites from being resolved. On the basis of previous studies,[32] the ^{51}V isotropic shift of the nanosheets of $V_2O_5 \cdot nH_2O$ suggested octahedral vanadium sites with one water

molecule bonded to the vanadyl oxygen or vanadium pentoxide with shifted subunits.

Notably, the integral intensity of the total ^{51}V signal including the spinning side band manifold of the $V_2O_5 \cdot nH_2O$ nanosheets was less than 20% of the V_2O_5 precursor. The broad line width of the side bands means that the second-order quadrupolar broadening cannot be measured from the line shape, and the contributions of the first-order quadrupolar interaction and shift anisotropy to the spinning side band manifold cannot be easily separated; consequently, the quadrupolar couplings were not measured.[34] One possible reason for the signal loss relative to the precursor would be a phase transition similar to that of $VO_2(M)$−metallic-$VO_2(R)$ because of frictional heating from MAS.[35,36]

The magnetic susceptibility data (see Figure S1) indicated a weak paramagnetic behavior of the nanosheets with no observable magnetic phase transition. A fit of these data returned a Weiss constant of zero, pure Curie paramagnetism which we ascribe to isolated (noninteracting) V^{4+} ions that were incorporated between the V_2O_5 nanosheets during the course of the reaction. In turn, we ascribe the large reduction in the observable signal from V_2O_5 to a paramagnetic bleaching effect, where the nuclear relaxation of V^{5+} is enhanced by the proximity of the paramagnetic V^{4+} ions.[27] As the synthesis was performed in an aqueous mixture of $VO_2(M)$ and V_2O_5, the former provided a possible source of paramagnetic V^{4+}, given the 1:4-fraction of $VO_2(M)$ and V_2O_5. $V_2O_5 \cdot nH_2O$ has been found to contain about 10 mol % of V^{4+} according to Etman et al.,[7] which was in agreement with the observed weakly paramagnetic behavior. The presence of V^{4+} was here confirmed by ESR (see Figure S2). The corresponding spectra each had a broad peak with an isotropic g-value of 1.95 at room temperature. This value matched well with those reported for other V^{4+}-containing materials.[23,29,37]

2.1.2. Water Molecules in $V_2O_5 \cdot nH_2O$ Nanosheets. The distribution and location of H_2O in $V_2O_5 \cdot nH_2O$ are important for the electrochemical behavior and semiconducting properties.[20,21] In relation to the positioning of H_2O, Pozarnsky and McCormick suggested a chain model with a H_2O molecule and a −OH group in the equatorial plane and an additional H_2O pointing downward.[25] Hence, we recorded a static ^2H ss-NMR spectrum (see Figure 3) on the $V_2O_5 \cdot nD_2O$ nanosheets and observed three distinct resonances with decreasing intensities at chemical shifts of 1, 3.3, and 7 ppm. Similar results were obtained from ^1H NMR experiments under MAS, but the ^1H background of the probe and rotor complicated the interpretation (data not shown). Takeda et al. have observed
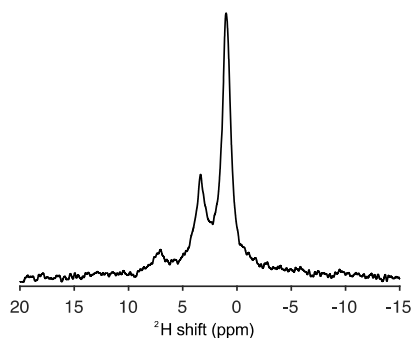
rotational restricted motion in hydrated V_2O_5 as evidenced by the features of the ^2H powder patterns.[22] In this work, neither bulk H_2O nor strongly coordinated H_2O could be observed. Instead, the features of the static ^2H spectrum suggested that H_2O had a high mobility. However, H_2O or −OH groups bonded or coordinated to V^{4+} were not easily detectable under static conditions, as they were expected to be strongly shifted by a Fermi-contact shift to the paramagnetic V^{4+} ion, exhibit large resonance broadening, and have short relaxation times. The observed ^2H chemical shifts at 3.3 and 1 ppm were attributed to D_2O and −OD on the surface of the nanosheets, respectively.[38] The chemical shift at 7 ppm may have been due to −OD groups, in which the O atom bridges between two V atoms.

2.2. Probing Nanosheet Formation by Real-Time ^{51}V NMR. To elucidate the formation of nanosheets, we applied real-time solid- and solution-state ^{51}V NMR to follow the reaction of the solid phases and the dissolved species separately.

2.2.1. Dissolved Species. VO_2 and V_2O_5 with a mass ratio of 1:4 were blended with 550 μL of H_2O and 50 μL of D_2O in an NMR tube, and solution-state ^{51}V NMR spectra were recorded in real time during the reaction. The observed vanadium species and their ^{51}V shift are summarized in Table 1. It was

Table 1. Dissolved Vanadium Species Observed with Solution-State NMR[a]

dissolved vanadium species	^{51}V shift (ppm)
$[H_2V_{10}O_{28}]^{4-}$	−419, −503, −522
$[VO_2 \cdot 4H_2O]^+$	−549

[a]The peak at −297 ppm could not be assigned.

evident that the ^{51}V signals of the decavanadate anion $[H_2V_{10}O_{28}]^{4-}$, resonating at −419, −503, and −522 ppm, exhibited increasing integral intensities for up to 2 h after mixing, whereas the ^{51}V signal of the hydrated dioxovanadate cation $[VO_2 \cdot 4H_2O]^+$ at −549 ppm retained a constant integral (see Figure 4). The decavanadate anion is believed to be produced from 10 dioxovanadate cations under acidic conditions in aqueous solutions. However, if this reaction had occurred here, there must also have been an additional process where dioxovanadate cations were produced. Fur-

Figure 3. Static ^2H NMR of $V_2O_5 \cdot nD_2O$ nanosheets. The ^2H NMR spectrum was recorded using a quadrupolar echo sequence.
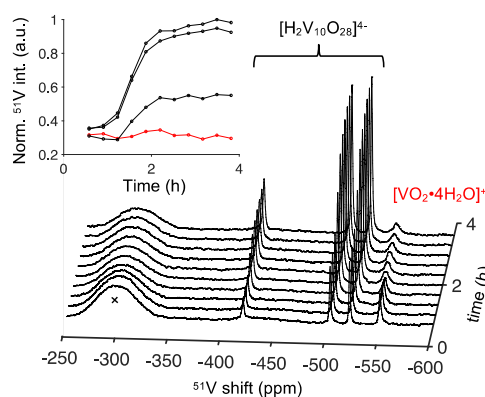
Figure 4. Stacked real-time solution-state NMR spectra as a function of time. "x" marks an unassigned peak. The inset shows the normalized ^{51}V signal integral as a function of time for $[H_2V_{10}O_{28}]^{4-}$ (black) and $[VO_2 \cdot 4H_2O]^+$ (red).
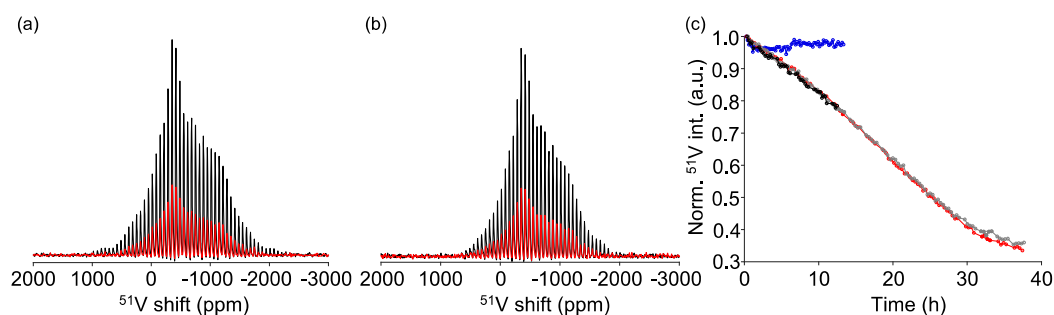
Figure 5. Low-flip-angle direct excitation (a) and Hahn echo (b) MAS ss-NMR spectra at 70 °C for the VO_2/V_2O_5 mass ratio of 1:4 extracted from real-time experiments at time = 0 (black trace) and time = 38 h (red trace). (c) Normalized ^{51}V integrals vs time for reactions with aged VO_2 (blue) or fresh VO_2 (Hahn echo red; direct excitation gray) in the reaction mixture. The black curve is a repetition using a Hahn echo.

thermore, the rate of its formation has to be equal to the rate of consumption, so as to keep the overall dioxovanadate concentration unaltered throughout the entire reaction. It has furthermore been discussed that the decavanadate anion is not responsible for the formation of the nanosheets because it is highly acidic and hence would prevent further condensation reactions.[39] Notably, a broad feature at a shift of about −297 ppm was observed (see Figure 4), which Rehder has suggested to be related to a VO_2^+ derivate.[40] The broadening of this ^{51}V signal might also be attributed to polymeric vanadium species or species that contain V^{4+} in close vicinity.

The dioxovanadate cation was exchanged with $H_2VO_4^-$, which has a pK_a of 3.8.[41] It is, hence, highly likely that the observed chemical shift of $[VO_2 \cdot 4H_2O]^+$ was due to an average of both the cationic and anionic forms and is highly pH-dependent. The observed chemical shift agreed well with the reported one at a pH of 3.8.[41] The formation of the decavanadate anion produces H^+, which lowered the pH to 2.6 at the end of the reaction, which in turn shifted the ^{51}V signal of the dioxovanadate cation from −550 ppm to less negative chemical shift values.

An aqueous suspension of VO_2 did not produce any ^{51}V NMR peaks at room temperature or 80 °C. Hence, we assumed that all of the ^{51}V signals (in Figure 4) including the broad peak at −297 ppm resulted from V_2O_5 and its reaction products despite its low solubility (0.7 g/L = 3.8 mmol/L at room temperature).[42] It is worth mentioning that VO_2 is, however, slightly water-soluble particularly under acidic conditions, and the following V^{4+} species, which are NMR silent, might be present: $[VO \cdot 5H_2O]^{2+}$, $VOOH^+$, and a dimer $VO_2(OH_2)^{2+}$; the latter most likely formed from the coupling of two $VOOH^+$ species.[43] V^{4+} species in an aqueous VO_2/V_2O_5 mixture at 80 °C was confirmed by the hyperfine coupling between an electron and ^{51}V in the ESR spectrum showing eight peaks (see Figure S2). These features of the ESR spectrum suggested isolated V^{4+} species in solution,[29] most likely $[VO \cdot 5H_2O]^{2+}$. Furthermore, the ESR spectrum had a broad feature, which was attributed to solid VO_2, and an aqueous mixture of solely V_2O_5 did not give any ESR signal.

The same vanadium species have been observed in preparations from other approaches using ion-exchange and sol−gel methods.[23−25,37] Our observations were consistent with findings from other synthetic methods taking into account the acidic conditions with pH = 3.8. Furthermore, the observed ^{51}V NMR signals agreed well with earlier findings on the concentration and pH dependence for vanadium species formed in aqueous solutions.[21]

Etman et al. have reported on an onset of the $V_2O_5 \cdot nH_2O$ formation after 90 min using real-time XRD,[7] while the formation of decavanadate leveled out after 2.5 h. By comparing those findings with the ones of this study, the question arose if the dissolved species were responsible for the formation of nanosheets or if the observations of the decavanadate anion and the dioxovanadate cation were solely due to various side reactions of the aqueous vanadium chemistry. Many mechanisms have been proposed for the formation of nanostructured gels,[23−25,37] and in our view, the most relevant are those that have dealt with ion exchange.[23,25] However, notably, all of them have derived these compounds from vanadium-based species in solution, whereas here we instead started from two commercial solid compounds (V_2O_5 and VO_2).

2.2.2. Solid Species. To access information on the solid phases during the reaction, we performed real-time MAS ss-NMR experiments on the reaction mixture (0.3 mg of VO_2, 1.2 mg of V_2O_5, and 20 μL of H_2O) at 7 kHz MAS. Analyses of the ^{51}V NMR spectra in Figure 5a,b showed a reduction of the integral of the whole ^{51}V signal spinning side band manifold due to the V_2O_5 phase, which has an isotropic chemical shift of −611 ppm. The reduction was observed both for low-flip-angle direct excitation (Figure 5c, gray) and in a Hahn echo experiment (Figure 5c, red). The normalized ^{51}V NMR integrals of a repeated Hahn echo experiment (Figure 5c, black) coincided well with the first reaction. Vanadium-containing compounds have a very large ^{51}V NMR shift range, which in turn required that we moved the observation window by changing the carrier frequency and retuning the probe to observe various species. By comparing weight-normalized ^{51}V MAS ss-NMR spectra of fresh commercial $VO_2(M)$ and V_2O_5, the observed broad ^{51}V signal of $VO_2(M)$ at approximately 2100 ppm[30] was consistent with <1% of the V_2O_5 signal in the solid phase (see Figure S3). This intensity was lower than expected and was ascribed to the broad ^{51}V resonance of VO_2 being harder to excite and having a shorter relaxation time than those of V_2O_5. The other ^{51}V signal resonating at negative shift is most likely the impurity V_2O_5 (see Figure S3). Consequently, an amount of approximately 0.3 mg of $VO_2(M)$ was undetectable in the real-time MAS ss-NMR experiments. The lab-scale synthesis was prepared under similar conditions as in real-time MAS ss-NMR experiment and revealed traces of unexfoliated V_2O_5 at the end of the synthesis, which agreed with the remaining signal in the ^{51}V NMR spectra detected after 38 h (see Figure 5c, red and gray), and was therefore attributed to this unexfoliated V_2O_5 precursor. Despite attempts to observe other ^{51}V signals, for

example, from VO_2, none were detected. One reason might have been the small rotor volume of 20 μL, which required a V_xO_y–H_2O ratio that is 17 times larger to assure a good signal-to-noise ratio and to minimize the uncertainty of the weighed amount of solids, as compared to the lab-scale synthesis. In total, approximately 1.5 mg of V_xO_y was present.

Interestingly, the synthesis of the $V_2O_5 \cdot nH_2O$ nanosheets failed when V_2O_5 was used solely as the precursor (data not shown), suggesting that $VO_2(M)$ or dissolved species formed from $VO_2(M)$ initiated the formation of the $V_2O_5 \cdot nH_2O$ nanosheets. A requirement of $VO_2(M)$ for this synthesis was proposed by Pozarnsky and McCormick who reported on the formation of V^{4+} species by ion exchange and the consumption of those during the reaction.[23,41] They suggested that $[V^{4+}O \cdot 5H_2O]^{2+}$ reacted with $[V^{5+}O_2 \cdot 4H_2O]^+$ and formed oligomeric species, which polymerized further. Hence, our observations of a reduction of the V_2O_5 signal during the course of the reaction might be explained by a homogeneous distribution of V^{4+} in close vicinity of V^{5+} formed via polymerization rather than the consumption of V_2O_5 into other species. Our proposed reaction pathway, which is in agreement with Pozarnsky and McCormick,[23,41] is illustrated in Figure 6. Alternatively, as
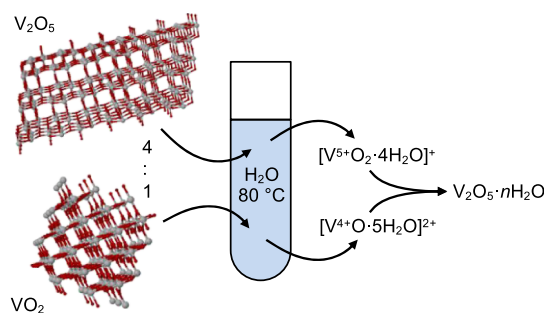

Figure 6. Proposed reaction pathways occurring during the synthesis of $V_2O_5 \cdot nH_2O$ nanosheets.

Livage discussed, $[V^{4+}O \cdot 5H_2O]^{2+}$ could intercalate between the V_2O_5 layers.[21] This alternative hypothesis would be possible if $[V^{4+}O \cdot 5H_2O]^{2+}$ would be homogeneously distributed.

It should also be noted that the synthesis reaction failed when aged $VO_2(M)$ was used (Figure 5c, blue). This aged compound had been stored under ambient conditions and was consequently altered after being in contact with air. To understand the reason behind this phenomenon, we compared the ^1H, ^{51}V NMR, ESR spectra, and XRD patterns of the fresh and aged $VO_2(M)$.

The XRD pattern of the fresh sample agreed well with the standard pattern of monoclinic $VO_2(M)$. By contrast, the XRD pattern of the aged sample had fewer peaks, which complicated the assignment of the formed VO_x phase (Figure S4). Interestingly, the semilogarithmic plot revealed 001 and 003 reflections of the $V_2O_5 \cdot nH_2O$ phase in the pattern of the aged $VO_2(M)$, which matched well with previous reports on the instability of $VO_2(M)$ under ambient conditions.[44] In comparison with the ^{51}V MAS ss-NMR spectrum of fresh $VO_2(M)$ (see Figure S3, red) in which broad peaks resonating between 1800 and 3000 ppm were attributed to $VO_2(M)$, the aged VO_2 showed no such peaks (see Figure S5, black), presumably due to oxidation of the vanadium species to V_2O_5. On the other hand, the ESR spectrum (see Figure S2) indicated that the aged VO_2 still possessed a reasonable

measurable quantity of V^{4+}. Furthermore, the ^1H NMR (data not shown) displayed a broad ^1H NMR peak for the aged $VO_2(M)$ as compared to the fresh one. The increased ^1H NMR signal intensity suggested strongly that concurrent H_2O uptake had occurred. Hence, as was reported by Etman et al.,[7] the relative fraction of $VO_2(M)$–V_2O_5 used in the synthesis was crucial for successful exfoliation.

3. CONCLUSIONS

To summarize, real-time solid-state and solution-state ^{51}V NMR studies were performed to follow the transformation of VO_2 and V_2O_5 in aqueous dispersion into nanosheets of $V_2O_5 \cdot nH_2O$. During exfoliation, a loss of the ^{51}V NMR signal of V_2O_5 was observed, which was attributed to a homogeneous distribution of V^{4+} that is in close contact with V^{5+} bleaching their signals. Taken together, our findings were consistent with a hypothesis that both V_2O_5 and VO_2 had been dissolved and VO_2 formed as $[V^{4+}O \cdot 5H_2O]^{2+}$ cations, which were oligomerized with $[V^{5+}O_2 \cdot 4H_2O]^+$ species from V_2O_5 and then polymerized further. Another explanation could have been intercalation of $[V^{4+}O \cdot 5H_2O]^{2+}$ between the layers of V_2O_5. Additional future studies could include real-time ESR experiments with stirring; however, such were out of the scope of this current study.

4. MATERIALS AND METHODS

4.1. Materials. The $V_2O_5 \cdot nH_2O$ or $V_2O_5 \cdot nD_2O$ nanosheets were synthesized as described in ref 7. In a typical synthesis, a mixture of 1:4 (weight ratio) of V_2O_4 (Fisher Scientific, UK) and V_2O_4 (Sigma-Aldrich, Germany, purity 99.9%), denoted by $VO_2(M)$, was used as the precursors. The mixture of oxides was dispersed in water or D_2O (CortecNet, 99.8%) by sonication for 10 min and then heated under reflux at 80–90 °C for 8–24 h. At the end of heating process, a greenish black suspension of $V_2O_5 \cdot nH_2O$ nanosheets was formed, which was then dried in air at 80 °C for 5 h to obtain the $V_2O_5 \cdot nH_2O$ nanosheets.

For the real-time ss-NMR experiments, 0.3 mg of VO_2, 1.2 mg of V_2O_5, and 20 μL of H_2O were placed in a Kel-F insert, which can be sealed with screws. After sealing, the mixture was sonicated for a minute. The insert was then placed in a 4 mm rotor, which was inserted into the spectrometer.

For the real-time solution-state NMR experiments, VO_2 and V_2O_5 with a mass ratio of 1:4 were blended with 550 μL of H_2O and 50 μL of D_2O. The synthesis was performed at 70 °C, and the sample tube was spun at 20 Hz.

4.2. Methods. ^{51}V MAS NMR data were acquired on 14.1 T (^{51}V Larmor frequency of −157.9 MHz) and 9.4 T (Larmor frequency of −105.2 MHz) Bruker AVANCE-III spectrometers equipped with a 4 mm or 3.2 mm triple-resonance MAS probe. Real-time MAS ^{51}V NMR spectra were recorded at a MAS rate of 7 kHz, while rotors containing solely solid compounds were spun at the rate of 14 or 24 kHz. The isotropic chemical shift was determined by comparing ^{51}V NMR spectra recorded at two different spinning frequencies. An aqueous solution of sodium metavanadate (1 mol/L) was used to externally calibrate the ^{51}V NMR chemical shift to −574.38 ppm.[45] For solid samples, the length and strength of the radio frequency (rf) pulse were estimated using the reference solution, and a rf pulse and a nominal flip angle of 10° were used for single pulse acquisition. For real-time MAS experiments on the reaction mixture, the rf pulse was calibrated

on the sample itself and a 45° nominal flip angle was used. Applied rf fields between 80 and 95 kHz and spectral widths between 2500 and 5000 kHz were used. The carrier frequency was placed on resonance at the isotropic shift for V_2O_5 as well at $VO_2(M)$ and others. The ^{51}V longitudinal relaxation time constants T_1 for the solid compounds were estimated to be less than a second at room temperature and at 85 °C. Nevertheless, a repetition delay of 5 s was used for the real-time MAS NMR measurements on the reaction mixture at 85 °C. Static ^2H NMR was carried out on $V_2O_5 \cdot nD_2O$ nanosheets prepared in D_2O instead of H_2O. A small piece of the $V_2O_5 \cdot nD_2O$ nanosheets was glued in place in a glass insert, which was inserted into the rotor. The ^2H NMR spectra were recorded without spinning, and a quadrupolar echo pulse sequence was used. For real-time solution-state NMR measurements, V_2O_5 and VO_2 with a mass ratio of 4:1 were blended with 550 μL of H_2O and 50 μL of D_2O in a 5 mm NMR tube. The synthesis was performed at 70 °C, and the sample tube was spun at 20 Hz.

A moderately wide Gaussian function, which was optimized to reach close to 0 at the time point the signal had decayed, was pairwise multiplied with the recorded free induction decays before Fourier transformation. Unless otherwise stated, the spectral intensities were normalized to the mass of the sample packed in the rotor. Processing including baseline corrections was performed with in-house scripts (MATLAB, Mathworks).

All ESR experiments were carried out on a Bruker ELEXYS (X-band) spectrometer at room temperature or 80 °C. Samples were studied in a glass capillary, and the magnetic field was stepped from 1000 to 6000 gauss using two or eight signal accumulations. For heat treatment, capillaries were flame sealed prior to storage in the oven at 80 °C.

XRD measurements were conducted in the 2θ range of 5°−45° using a PANalytical diffractometer (Cu $K\alpha1$ radiation) and a synchrotron source (SLS beamline, λ = 0.7766 Å). The morphology of the nanosheets and their SAED patterns were studied by a transmission electron microscope (JEOL JEM-2100LaB$_6$) using an accelerating voltage of 200 kV.

pH measurements were performed with a Hanna instrument (model-HI2210). A Quantum Design MPMS XL SQUID (superconducting quantum interference device) magnetometer was used for magnetic characterization. Magnetization versus temperature measurements in a magnetic field of 1 kOe were performed in the temperature range of 2−107 K in steps of 3 K.

ASSOCIATED CONTENT

$\mathbf{S}$ Supporting Information

The Supporting Information is available free of charge on the ACS Publications website at DOI: 10.1021/acsomega.9b00727.

Variation of magnetic susceptibility with temperature, ESR spectra, weight-normalized ^{51}V MAS ss-NMR spectra of V_2O_5 and VO_2, XRD patterns of VO_2 fresh and aged, and ^{51}V MAS ss-NMR spectra of the aged VO_2 (PDF)

AUTHOR INFORMATION

Corresponding Authors

*E-mail: junliang.sun@pku.edu.cn (J.S.).
*E-mail: diana.bernin@chalmers.se (D.B.).

ORCID

Ahmed S. Etman: 0000-0003-0358-2379
Andrew J. Pell: 0000-0002-2542-8113
Niklas Hedin: 0000-0002-7284-2974
Xiaodong Zou: 0000-0001-6748-6656
Junliang Sun: 0000-0003-4074-0962
Diana Bernin: 0000-0002-9611-2263

Present Address

#Department of Physics, Chemistry and Biology (IFM), Linköping University, 581 83, Linköping, Sweden.

Notes

The authors declare no competing financial interest.

ACKNOWLEDGMENTS

REFERENCES

(1) Tan, C.; Cao, X.; Wu, X.-J.; He, Q.; Yang, J.; Zhang, X.; Chen, J.; Zhao, W.; Han, S.; Nam, G.-H.; et al. Recent Advances in Ultrathin Two-Dimensional Nanomaterials. *Chem. Rev.* **2017**, *117*, 6225−6331.

(2) Choi, W.; Choudhary, N.; Han, G. H.; Park, J.; Akinwande, D.; Lee, Y. H. Recent development of two-dimensional transition metal dichalcogenides and their applications. *Mater. Today* **2017**, *20*, 116−130.

(3) Etman, A. S.; Wang, L.; Edström, K.; Nyholm, L.; Sun, J. Molybdenum Oxide Nanosheets with Tunable Plasmonic Resonance: Aqueous Exfoliation Synthesis and Charge Storage Applications. *Adv. Funct. Mater.* **2019**, *29*, 1806699.

(4) Wang, Y.; Zhang, Z.; Zhu, Y.; Li, Z.; Vajtai, R.; Ci, L.; Ajayan, P. M. Nanostructured VO_2 Photocatalysts for Hydrogen Production. *ACS Nano* **2008**, *2*, 1492−1496.

(5) Etman, A. S.; Asfaw, H. D.; Yuan, N.; Li, J.; Zhou, Z.; Peng, F.; Persson, I.; Zou, X.; Gustafsson, T.; Edström, K.; et al. A One-Step Water Based Strategy for Synthesizing Hydrated Vanadium Pentoxide Nanosheets from $VO_2(B)$ as Free-Standing Electrodes for Lithium Battery Applications. *J. Mater. Chem. A* **2016**, *4*, 17988−18001.

(6) Etman, A. S.; Sun, J.; Younesi, R. $V_2O_5 \cdot nH_2O$ Nanosheets and Multi-Walled Carbon Nanotube Composite as a Negative Electrode for Sodium-Ion Batteries. *J. Energy Chem.* **2019**, *30*, 145−151.

(7) Etman, A. S.; Inge, A. K.; Jiaru, X.; Younesi, R.; Edström, K.; Sun, J. A Water Based Synthesis of Ultrathin Hydrated Vanadium Pentoxide Nanosheets for Lithium Battery Application: Free Standing Electrodes or Conventionally Casted Electrodes? *Electrochim. Acta* **2017**, *252*, 254−260.

(8) Bao, J.; Zhang, X.; Bai, L.; Bai, W.; Zhou, M.; Xie, J.; Guan, M.; Zhou, J.; Xie, Y. All-Solid-State Flexible Thin-Film Supercapacitors with High Electrochemical Performance Based on a Two-Dimensional $V_2O_5 \cdot H_2O$/Graphene Composite. *J. Mater. Chem. A* **2014**, *2*, 10876−10881.

(9) Qian, A.; Zhuo, K.; Shin, M. S.; Chun, W. W.; Choi, B. N.; Chung, C.-H. Surfactant Effects on the Morphology and Pseudocapacitive Behavior of $V_2O_5 \cdot H_2O$. *ChemSusChem* **2015**, *8*, 2399−2406.

(10) Yan, Y.; Li, B.; Guo, W.; Pang, H.; Xue, H. Vanadium Based Materials as Electrode Materials for High Performance Supercapacitors. *J. Power Sources* **2016**, *329*, 148−169.

(11) Rui, X.; Lu, Z.; Yin, Z.; Sim, D. H.; Xiao, N.; Lim, T. M.; Hng, H. H.; Zhang, H.; Yan, Q. Oriented Molecular Attachments Through Sol-Gel Chemistry for Synthesis of Ultrathin Hydrated Vanadium Pentoxide Nanosheets and Their Applications. *Small* **2013**, *9*, 716−721.

(12) Liu, L.; Yao, T.; Tan, X.; Liu, Q.; Wang, Z.; Shen, D.; Sun, Z.; Wei, S.; Xie, Y. Room-Temperature Intercalation-Deintercalation

Strategy towards $VO_2(B)$ Single Layers with Atomic Thickness. *Small* **2012**, *8*, 3752–3756.

(13) Rui, X.; Lu, Z.; Yu, H.; Yang, D.; Hng, H. H.; Lim, T. M.; Yan, Q. Ultrathin V_2O_5 Nanosheet Cathodes: Realizing Ultrafast Reversible Lithium Storage. *Nanoscale* **2013**, *5*, 556–560.

(14) Zhang, C.; Park, S.-H.; O'Brien, S. E.; Seral-Ascaso, A.; Liang, M.; Hanlon, D.; Krishnan, D.; Crossley, A.; McEvoy, N.; Coleman, J. N.; et al. Liquid Exfoliation of Interlayer Spacing-Tunable 2D Vanadium Oxide Nanosheets: High Capacity and Rate Handling Li-Ion Battery Cathodes. *Nano Energy* **2017**, *39*, 151–161.

(15) McNulty, D.; Buckley, D. N.; O'Dwyer, C. Synthesis and Electrochemical Properties of Vanadium Oxide Materials and Structures as Li-Ion Battery Positive Electrodes. *J. Power Sources* **2014**, *267*, 831–873.

(16) Dai, Y.; Li, Q.; Tan, S.; Wei, Q.; Pan, Y.; Tian, X.; Zhao, K.; Xu, X.; An, Q.; Mai, L.; et al. Nanoribbons and Nanoscrolls Intertwined Three-Dimensional Vanadium Oxide Hydrogels for High-Rate Lithium Storage at High Mass Loading Level. *Nano Energy* **2017**, *40*, 73–81.

(17) Liu, D.; Liu, Y.; Garcia, B. B.; Zhang, Q.; Pan, A.; Jeong, Y.-H.; Cao, G. V_2O_5 Xerogel Electrodes with Much Enhanced Lithium-Ion Intercalation Properties with N_2 Annealing. *J. Mater. Chem.* **2009**, *19*, 8789–8795.

(18) West, K.; Zachau-Christiansen, B.; Jacobsen, T.; Skaarup, S. Vanadium Oxide Xerogels as Electrodes for Lithium Batteries. *Electrochim. Acta* **1993**, *38*, 1215–1220.

(19) Su, D.; Wang, G. Single-Crystalline Bilayered V_2O_5 Nanobelts for High-Capacity Sodium-Ion Batteries. *ACS Nano* **2013**, *7*, 11218–11226.

(20) Moretti, A.; Passerini, S. Bilayered Nanostructured $V_2O_5 \cdot n\, H_2O$ for Metal Batteries. *Adv. Energy Mater.* **2016**, *6*, 1600868.

(21) Livage, J. Vanadium Pentoxide Gels. *Chem. Mater.* **1991**, *3*, 578–593.

(22) Takeda, S.; Gotoh, Y.; Maruta, G.; Takahara, S.; Kittaka, S. Restricted Rotational Motion of InterlayerWaterMolecules in Vanadium Pentoxide Hydrate, $V_2O_5 \cdot nD_2O$, as Studied by Deuterium NMR. *Z. Naturforsch., A: Phys. Sci.* **2002**, *57*, 419–424.

(23) Pozarnsky, G. A.; McCormick, A. V. ^{51}V NMR and EPR Study of Reaction Kinetics and Mechanisms in V_2O_5 Gelation by Ion Exchange of Sodium Metavanadate Solutions. *Chem. Mater.* **1994**, *6*, 380–385.

(24) Fontenot, C. J.; Wiench, J. W.; Pruski, M.; Schrader, G. L. Vanadia Gel Synthesis via Peroxovanadate Precursors. 1. In Situ Laser Raman and ^{51}V NMR Characterization of the Gelation Process. *J. Phys. Chem. B* **2000**, *104*, 11622–11631.

(25) Pozarnsky, G. A.; McCormick, A. V. ^{17}O Nuclear Magnetic Resonance Spectroscopy of the Structural Evolution of Vanadium Pentaoxide Gels. *J. Mater. Chem.* **1994**, *4*, 1749–1753.

(26) Alonso, B.; Livage, J. Synthesis of Vanadium Oxide Gels from Peroxovanadic Acid Solutions: A ^{51}V NMR Study. *J. Solid State Chem.* **1999**, *148*, 16–19.

(27) Shubin, A. A.; Lapina, O. B.; Courcot, D. Characterization by Solid State ^{51}V NMR Spectroscopy. *Catal. Today* **2000**, *56*, 379–387.

(28) Pell, A. J.; Pintacuda, G.; Grey, C. P. Paramagnetic NMR in Solution and the Solid State. *Prog. Nucl. Magn. Reson. Spectrosc.* **2019**, *111*, 1–271.

(29) Brückner, A. In situ electron paramagnetic resonance: a unique tool for analyzing structure-reactivity relationships in heterogeneous catalysis. *Chem. Soc. Rev.* **2010**, *39*, 4673–4684.

(30) Hope, M. A.; Griffith, K. J.; Cui, B.; Gao, F.; Dutton, S. E.; Parkin, S. S. P.; Grey, C. P. The Role of Ionic Liquid Breakdown in the Electrochemical Metallization of VO_2: An NMR Study of Gating Mechanisms and VO_2 Reduction. *J. Am. Chem. Soc.* **2018**, *140*, 16685–16696.

(31) Chernova, N. a.; Roppolo, M.; Dillon, A. C.; Whittingham, M. S. Layered Vanadium and Molybdenum Oxides: Batteries and Electrochromics. *J. Mater. Chem.* **2009**, *19*, 2526.

(32) Fontenot, C. J.; Wiench, J. W.; Pruski, M.; Schrader, G. L. Vanadia Gel Synthesis via Peroxovanadate Precursors. 2. Characterization of the Gels. *J. Phys. Chem. B* **2001**, *105*, 10496–10504.

(33) Doublet, M.-L.; Lepetit, M.-B. Leading Interactions in the β-SrV_6O_{15} Compound. *Phys. Rev. B: Condens. Matter Mater. Phys.* **2005**, *71*, 075119.

(34) Skibsted, J.; Nielsen, N. C.; Bildsøe, H.; Jakobsen, H. J. Satellite Transitions in MAS NMR Spectra of Quadrupolar Nuclei. *J. Magn. Reson.* **1991**, *95*, 88–117.

(35) Gro Nielsen, U.; Skibsted, J.; Jakobsen, H. J. β-VO_2—a V(IV) or a Mixed-Valence V(III)−V(V) Oxide—Studied by ^{51}V MAS NMR Spectroscopy. *Chem. Phys. Lett.* **2002**, *356*, 73–78.

(36) Leroux, C.; Nihoul, G.; Van Tendeloo, G. From $VO_2(B)$ to $VO_2(R)$: Theoretical Structures of VO_2 Polymorphs and in Situ Electron Microscopy. *Phys. Rev. B: Condens. Matter Mater. Phys.* **1998**, *57*, 5111–5121.

(37) Bouhedja, L.; Steunou, N.; Maquet, J.; Livage, J. Synthesis of Polyoxovanadates from Aqueous Solutions. *J. Solid State Chem.* **2001**, *162*, 315–321.

(38) Nedumkandathil, R.; Jaworski, A.; Grins, J.; Bernin, D.; Karlsson, M.; Eklöf-Österberg, C.; Neagu, A.; Tai, C.-W.; Pell, A. J.; Häussermann, U. Hydride Reduction of $BaTiO_3$−Oxyhydride Versus O Vacancy Formation. *ACS Omega* **2018**, *3*, 11426–11438.

(39) Livage, J. Hydrothermal Synthesis of Nanostructured Vanadium Oxides. *Materials* **2010**, *3*, 4175–4195.

(40) Rehder, D. Vanadium NMR of Organovanadium Complexes. *Coord. Chem. Rev.* **2008**, *252*, 2209–2223.

(41) Pettersson, L.; Hedman, B.; Nenner, A.-M.; Andersson, I.; Hoyer, E. Multicomponent Polyanions. 36. Hydrolysis and Redox Equilibria of the H^+-HVO_4^{2-} System in 0.6 M Na(Cl). A Complementary Potentiometric and ^{51}V NMR Study at Low Vanadium Concentrations in Acid Solution. *Acta Chem. Scand.* **1985**, *39a*, 499–506.

(42) Lide, D. R. *CRC Handbook of Chemistry and Physics*, Internet Version 2005; CRC Press: Boca Raton, FL, 2005.

(43) Kustin, K. Aqueous Vanadium Ion Dynamics Relevant to Bioinorganic Chemistry: A Review. *J. Inorg. Biochem.* **2015**, *147*, 32–38.

(44) Occhiuzzi, M.; Cordischi, D.; Dragone, R. Reactivity of Some Vanadium Oxides: An EPR and XRD Study. *J. Solid State Chem.* **2005**, *178*, 1551–1558.

(45) Nielsen, U. G.; Hazell, A.; Skibsted, J.; Jakobsen, H. J.; McKenzie, C. J. Solid-State ^{51}V MAS NMR Spectroscopy Determines Component Concentration and Crystal Phase in Co-Crystallised Mixtures of Vanadium Complexes. *CrystEngComm* **2010**, *12*, 2826.